Journal of Materials Chemistry A

Accepted Manuscript

ROYAL SOCIETY OF CHEMISTRY

www.rsc.org/materialsA

Journal of Materials Chemistry A

PAPER

"Nanotraps" in porous electrospun fibers for effective removal of lead(II) in water

Received 00th January 20xx,
Accepted 00th January 20xx

DOI: 10.1039/x0xx00000x

www.rsc.org/

Anitha Senthamizhan,*[‡a] Brabu Balusamy,[‡a] Asli Celebioglu[a] and Tamer Uyar*[a,b]

Here, we have put in a conscientious effort to demonstrate how careful design of binding sites in the fibers and their stability for enhanced adsorption of metal ions, which has proven to be challenging task until now. The dithiothreitol capped gold nanoclusters (AuNC) are successfully encapsulated into a cavity in the form of pores in electrospun porous cellulose acetate fibers (pCAF) and their assembly creating a "nanotrap" for effective capturing of Pb^{2+}. The enhanced immobilization capacity of AuNC into interiors of the fibers and their non-aggregated nature offers enhanced adsorption sites, thus reaching maximum extraction capacity up to 1587 mg/g for Pb^{2+}. The interesting finding from this approach has shown that the diffusion of Pb^{2+} into the AuNC encapsulated porous cellulose acetate fiber (pCAF/AuNC) is in the similar passion with penetration depth of AuNC. The effectiveness of pCAF/AuNC has been compared with AuNC decorated non-porous cellulose acetate fiber (nCAF/AuNC). The findings have shown a remarkable improvement in the adsorption efficiency by increasing the availability and stability of adsorption sites in pCAF/AuNC. We strongly believe that the proposed approach might provide a new insight into developing a nanotraps to get rid of usual limitations including denaturation of adsorbent on supported matrix.

Introduction

Rapid development of global industrial activities have caused the increased release of heavy metal ions into water bodies, affecting human health and the environmental safety due to their toxic and carcinogenic nature even at very low concentration.[1-3] The removal of toxic metal ions and accessibility of clean water remains to be a critical challenge to mankind in the current scenario, expected to increase in the near future. This has necessitated the need for effective removal of toxic metal ions. Until now, various techniques have been adopted for the successful removal of heavy metal ions from polluted water, which include membrane separation, chemical precipitations, ion exchange, reverse osmosis, adsorption and so forth.[4-8] Precisely, adsorption is considered to be the most effectual method owing to its low cost, good performance, trouble-free operation, and its attribute to use a variety of materials as adsorbent.[9-13] Although nanoparticles play an active role in removing these metal ions, their practical applicability in waste water treatment is limited due to the need of additional separation procedures to recycle them from water.[14-17] In order to evade these issues, supported matrices have been introduced, due to which electrospun fibers have emerged as successful family of sorbents for removing heavy metal ions in the recent past.[18-23]

The most critical problem encountered in adsorbents including nanofibers is their limited adsorption capacity due to the adsorption of metal ions on their surface as monolayers and denaturation of adsorbent. It is known that the adsorption behavior is based on the functional groups present on the surface of adsorbents, which form a complex with heavy metal ions. Therefore, the adsorbent is expected to showcase high porosity, large surface area, and strong binding-site accessibility for adsorbates to result in rapid removal and high adsorption capacity.[24-30] As an example, the recent study by Zhenghui Li *et al*. has proved that the advantage of porous structure for excellent adsorption of organic pollutants in water.[31] The recent past has seen extensive research on the interaction of toxic pollutants with monolayer-protected metal nanoclusters (MNC) for the advanced development of better sensing procedure. This has seen the emergence of MNC to act as an efficient platform for new generation of sensing tools.[32-36]

The performance of the sensor is solely based on the changes in the properties of the gold core or the monolayer. In both cases, MNC stability forms the crux due to its sensitivity towards the environment. Recently, we have devised an effective method for integrating MNC with nanofibers and further studying their sensing performance.[37-39] The rapid adsorption ability of the metal ions on the surface of the MNC

[a] UNAM-National Nanotechnology Research Center, Bilkent University, Ankara, 06800, Turkey
[b] Institute of Materials Science & Nanotechnology, Bilkent University, Ankara, 06800, Turkey
TU: uyar@unam.bilkent.edu.tr
AS: senthamizhan@unam.bilkent.edu.tr
† Electronic Supplementary Information (ESI) available: BET results, SEM images, XPS Spectra, photographs, UV spectra and EDX mapping. See DOI: 10.1039/x0xx00000x
‡ These authors contributed equally to the research.

instigated us to further study the removal performance of metal ions from water. However, a major setback in achieving this goal is the protection of the functionalities of the MNC. The last few years have seen various studies for the decoration of the nanoparticles onto the electrospun fiber surface for various applications including sensors.[40-47] In such a case, usually include the incorporation of nanoparticles into fibers or decorate them on the surface as monolayer or multilayer resulting in nanoparticles/polymer composites. Interestingly, the incorporation of the nanoparticles inside the polymer fiber leads to protections of their stability while their concrete performance might be degraded.[48,49] In order to overcome this circumstance, the particles are decorated on the outer surface of the fibers, resulting in enhanced performance, while the protection of nanoparticles against the environment is under question.

In our case, the presence of ligands on the nanoclusters plays a vital role in binding with target metal pollutants. Under the condition where the nanoclusters are decorated on the fiber surface, the rate of exposure is found to be higher and the ligands on the gold surface are subjected to environmental degradation, might be expected to reduce removal efficiency. Additionally, the aggregation of MNC also has an impact on the removal performance owing to limited interaction with the pollutant at surface level. Thus, special attention needs to be paid to shield the MNC against the environment because of their sensitive surface. It is general assumption that adsorbed metal ions found on the MNC disable them by either removing the ligands or changing their chemical nature upon interaction with metal ions. Such cases prove aggregation of nanocluster to be unavoidable, leading to decreased adsorption performance. Based on the aforementioned points, we have worked towards finding a system to protect MNC on their fiber surface for easy accessibility. Concern has also been put on the selected MNC should not lose their activity upon interaction with metal ions. Based on literature, parameters for achieving high adsorption capacity include a large surface area, porous structure, enhanced acceptability of functional groups to the pollutants and stability. During last few decades, electrospinning approach has acknowledged a great deal of attention due to its simplicity, cost effectiveness, feasibility and scalability for production of nanofibers from diverse of materials.[50-52] Electrospun fibers possess several unique properties including high surface area, porous structure and flexibility which make them more attractive in variety of applications such as sensors, adsorbents, catalyst, filters and tissue regeneration.[53-56] We strongly apprehend and believe that these criteria thoroughly match the requirement of the current study.

This research work highlights our preliminary efforts to devise a synthetic strategy for the effective removal of Pb^{2+} in water by creating stable "nanotraps" in electrospun porous cellulose acetate fibers (pCAF). The resultant nanotraps enable higher uptake capacities of Pb^{2+} upto 1587 mg/g.

Experimental Section

Materials

Tetrachloroauric acid trihydrate ($HAuCl_4.3H_2O$), dichloromethane (DCM, ≥99% (GC)), methanol (≥99.7% (GC)), acetone (≥99% (GC)) cellulose acetate, (CA, Mw: 30000 g/mol, 39.8wt.% acetyl), zinc acetate dihydrate (~98%), lead (II) nitrate (99.0%) manganese (II) acetate tetrahydrate (99%) and nickel(II) acetate tetrahydrate (99.0%) were procured from Sigma-Aldrich. 1,4-Dithiothreitol (DTT), cadmium nitrate tetrahydrate and mercury (II) acetate were obtained from VWR Chemicals, Fluka and Merck, respectively. All chemicals were used as received without any further purification. Millipore Milli-Q Ultrapure Water System was used to acquire deionized water.

Electrospinning of porous and nonporous cellulose acetate fibers

The electrospun porous cellulose acetate fibers (pCAF) and nonporous cellulose acetate fibers (nCAF) were prepared by following the method reported earlier.[57] The process involves the preparation of homogenous polymer solution (10% w/v) by dissolving cellulose acetate (CA) in a binary solvent mixture of DCM and acetone at 1:1 volume ratio. In a similar fashion, nCAF was fabricated from the CA polymer solution which was prepared by dissolving CA at 12% (w/v) in a DCM and methanol binary solvent mixture (4/1 v/v). The resulting polymer solution was subjected to electrospinning at a flow rate of 0.5-1 mL/h using a syringe pump (KDS-101, KD Scientific, USA) and a 3 mL syringe hold 27 gauge metallic needle as spinneret under an optimized high voltage (10-15 kV) applied between the needle and grounded collector by high-voltage power supply (Spellman, SL30, USA). Then, an aluminium foil was used to cover the grounded metal plate for collecting the pCAF and nCAF which was located at a distance of 10-12 cm from the needle. The electrospinning process was performed at 23°C at 18% relative humidity in a Plexiglas box. The resulting pCAFM and nCAFM were further air dried in a fume hood at room temperature.

Synthesis of DTT capped gold nanoclusters (AuNC)

The DTT capped gold nanoclusters (AuNC) were prepared as described by Ding *et al.*[58] Briefly, 11 mg of DTT was dissolved in 10 mL deionized water under vigorous stirring. This was followed by immediate addition of 768 µL of $HAuCl_4$ solution at room temperature. Then, stirring was allowed for 3 minutes, followed by the addition of aqueous sodium hydroxide to reach pH 8. The resulting solution was subjected to further stirring for 6 h to obtain a colorless solution. Under UV irradiation (λ_{ext}-254 nm), the prepared AuNC emitted red fluorescence and further the clusters will be encapsulated into pCAF and nCAF.

Preparation of AuNC encapsulated pCAFM and nCAFM (pCAFM/AuNC and nCAFM/AuNC)

The method for encapsulation of AuNC into the pCAFM and nCAFM were performed by following our previous protocols.[59] The first step involves immersing pCAFM and nCAFM in AuNC solution separately for 3 h in a shaking platform, followed by carefully removing them from the solution and subjected to

drying at room temperature. Rinsing the membrane for around 15 minutes under vigorous shaking and then air drying them at room temperature removes the excess adsorbed clusters and ligands on the fiber surface.

Analytical procedure for preparation of metal ion stock solution

Stock solution (50 ppm) of Pb^{2+} was prepared by dissolving lead (II) nitrate salt in deionized water. Consequently, the desired concentrations of Pb^{2+} were prepared by diluting appropriate volume of the stock solution. Similarly, the same protocol was followed for solutions of Cd^{2+}, Zn^{2+}, Ni^{2+}, $Mn^{2+}$and Hg^{2+}.

Adsorption of toxic metal ions

Batch adsorption experiments were carried out to evaluate the removal efficiency of pCAFM/AuNC for toxic metal ions (Pb^{2+}, Cd^{2+}, Zn^{2+}, Ni^{2+}, $Mn^{2+}$and Hg^{2+}) in water. In a typical experiment, the membrane was placed (30 mg/mL) in a beaker containing metal ion solution (50 mL) followed by agitation at 100 rpm on a mechanical shaker under ambient conditions. The effect of contact time on removal performance of pCAFM/AuNC for Pb^{2+} ion was analyzed by withdrawing the samples at an arbitrary time period, ranging from 0 - 24 h, from a solution concentration of 1 ppm and 5 ppm, respectively. The pCAFM was used as the control for comparing the removal efficiency. Lastly, similar conditions were followed for investigating the effect of concentration (50 ppb to 5 ppm) on the removing performance. A similar procedure was carried out for nCAFM/AuNC also.

The removal efficiency and adsorption capacity (q_e, mg/g) of pCAFM/AuNC were calculated using the following equations.

$$\text{Removal efficiency (\%)} = \frac{(C_0 - C_e)}{C_0} \times 100$$

$$\text{Adsorption capacity } (q_e) = \frac{(C_0 - C_e) \times V}{m}$$

q_e is the adsorption amount (mg/g), C_0 and C_e are the concentration of metal ions in the aqueous solution before and after the adsorption, respectively (mg/L), V is the volume of the solution (L), and m is the weight of pCAFM/AuNC (g).

Instrumentation

Transmission electron microscope (TEM, Tecnai G2 F30) equipped with an EDS was employed to study the morphological and porous nature of the fibers. STEM-EDX (scanning transmission electron microscopy-energy dispersive X-ray analysis) was used to examine gold nanoclusters and metal ions on surface of fibers. The removal efficiencies of the nanofibers were determined by measuring the residual concentration of metal ions using inductively coupled plasma mass spectroscopy (ICP-MS, Thermo, X Series II). X-ray photoelectron spectroscopy (XPS, Thermo K-alpha-monochromated) was used to confirm the adsorbed metal ion on the surface of fibers and their chemical state. Contact angle measurements were carried out using contact-angle meter (OCA 30, Dataphysics). UV-Vis-NIR Spectrophotometer (Cary 100) was used to record the absorbance spectra. The surface area and pore size of the fibrous membrane were obtained using Brunauer Emmett and Teller (BET) surface area analyzer (Micromeritics TriStar 3000). The data were collected at 77K in the range of 0.1 - 0.9 relative pressure.

Results and discussion

The present study aims at designing a method for creating nanotraps by encapsulating dithiothreitol capped gold nanocluster (AuNC) with an average size of 2-3 nm into the electrospun porous cellulose acetate fibers (pCAF), named as pCAF/AuNC and enhancing more active sites by loading higher amount of AuNC into the porous fibers. In this approach, we have fabricated pCAF (diameter ~1-1.5 µm) with average pore size of 30-40 nm using simple and versatile single step electrospinning technique by playing the solvent and their composition of DCM/acetone (1/1 (v/v)). The attained porous structure in pCAF might be due the rapid evaporation of the highly volatile solvents (DCM and acetone) as compared with nCAF, with a consequent solidification of polymer chains as reported by our earlier publication.[57] To the best of our knowledge, no effort has been put on the metal ion removal performance, although the sensing characteristics of AuNC are well known.[58,59] Interestingly, we have been motivated by the specific characteristic of DTT to form a stable complex with metal ions using both of its sulfur donors.[60-62] When the pCAF are immersed into the AuNC solution, the pores in the fibers get swelled up, facilitating the transportation of AuNC into the fiber interior. Further, they can effectively bind on the pore walls by the formation of hydrogen bonding between them.

The excess amount of unbounded clusters on the fiber surface is carefully washed out immediately after drying the membrane. This is done to prevent the blockage of pores which might hamper the penetration of analytes into the fiber interiors. Also, it is believed that the diffusion of AuNC inside the pCAF facilitates further entry of AuNC from the solution into the interior of the porous fiber. The TEM image of pCAF/AuNC highlights the penetration of AuNC into interiors of the pCAF upto ~300 nm in depth as depicted in Fig. 1a, wherein the nanoclusters are well dispersed rather than aggregates on the external surface of the fibers. Expectedly, a cavity in the form of the fiber pores protects the properties of AuNC against the environment for prolonged time period. Also, we can observe the uniform penetration of the encapsulated AuNC into the fiber matrix, firmly anchored on their surface which can act as nanotraps for capturing toxic metal ions in water as demonstrated in Fig. 1a-b. The inset in Fig. 1b represents the high resolution TEM image of the AuNC showing lattice spacing of 0.235 nm which corresponds to (111) lattice plane of the face-centered cubic (fcc) gold.[63] The STEM image of the pCAF/AuNC confirms that the porous nature of pCAF are highly persistent and do not degrade following the incorporation of AuNC which is expected to enhance the rapid diffusion and fast response with heavy metal ions as seen Fig. 1c.

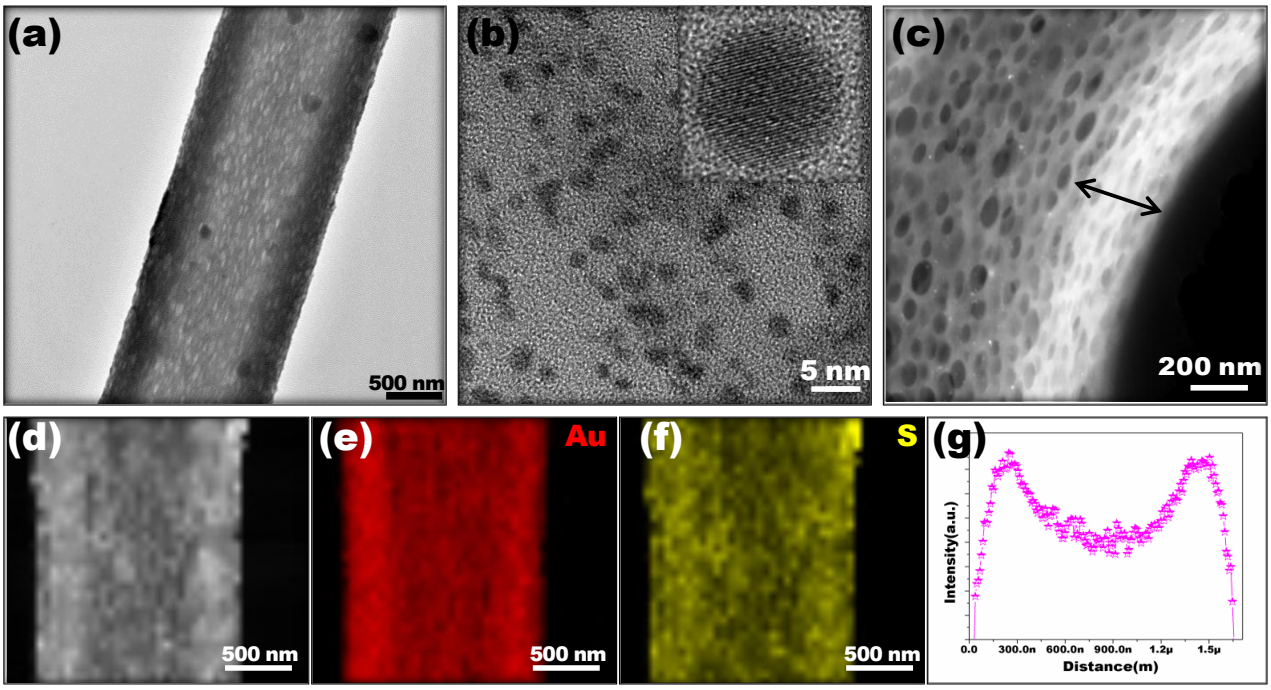

Fig. 1 (a) TEM image of gold nanocluster (AuNC) encapsulated porous cellulose acetate fiber (pCAF/AuNC). The image clearly demonstrates the penetration depth is almost uniform throughout the fiber, confirming the deep penetration of AuNC into the fiber interior. (b) TEM image of AuNC. The inset shows AuNC having lattice spacing of 0.235 nm which corresponds to (111) lattice plane of the face-centered cubic (fcc) gold. (c-d) HAADF-STEM image and EDS elemental mapping of (e) Au and (f) S. The image confirming the porous nature of the fiber is highly persistent and do not degrade following the incorporation of AuNC. (g) EDS intensity line profile of Au taken across the pCAF/AuNC surface.

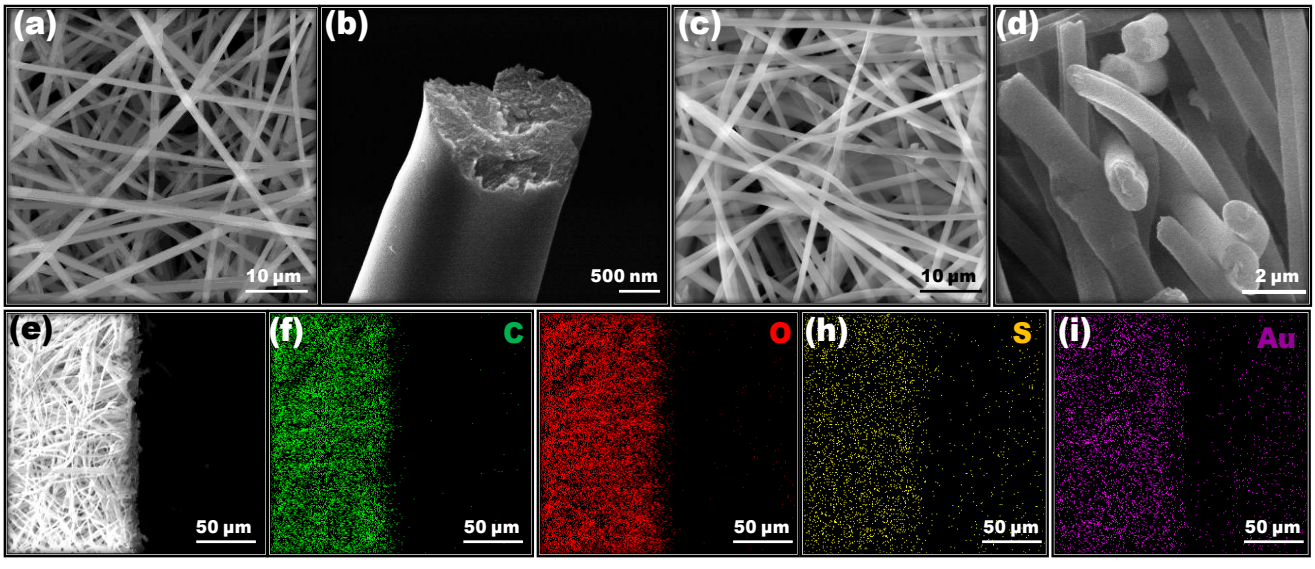

Fig. 2 SEM image and their cross sectional view of (a-b) nCAF and (c-d) nCAF/AuNC, confirming their nonporous nature. (e) SEM image and EDX mapping of nCAFM/AuNC (f) C (g) O (h) S and (i) Au. The uniform distribution of decorated AuNC over the fibrous membrane is clearly seen.

The size of the AuNC and pores in pCAF are considered to be an important factors for incorporation. It would be highly appreciated if the AuNC are smaller than the pores for effectual incorporation, to prevent blockage of the pore wall.

The above discussed facts have aided us in optimized the dipping time as 3 h for the successful incorporation of AuNC into pCAF under shaker. The uniform distribution of AuNC in the pCAF is confirmed by STEM-EDX elemental mapping as

depicted in Fig. 1d-f. The line intensity profile in Fig. 1g further confirms the penetration of AuNC is uniform along fibers. However, a question arises on whether the creation of nanotraps will dominate the removal efficiency of toxic metal ions or not. To confirm this, non-porous cellulose acetate fibers (nCAF) were decorated with AuNC which is named as nCAF/AuNC and their potency in metal ion removal was systematically compared with pCAF/AuNC. Fig. 2a and c shows the SEM image of nCAF before and after decorating with AuNC with an average diameter of 1 μM ± 280 nm and 1.3μM ± 250 nm, respectively. Compelling confirmation has been obtained from the cross sectional observation of nCAF about their solid nature as shown in Fig. 2b and d. The energy dispersive X-ray (EDX) elemental mapping of nCAF/AuNC demonstrates the uniform distribution of decorated AuNC over the fibrous membrane as depicted in Fig. 2e-i. The comparative surface area and pore size of nCAFM and pCAFM is given in Table S1. The specific surface area of the nCAFM and pCAFM were determined to be 3.36 and 9.73 m^2/g, respectively. The average pore size of the respective fibers were found to be 6.2 and 12.5 nm. After encapsulating with AuNC, the pAFM/AuNC shows the slight decreases in their surface area and pore size which observed as 6.89 m^2/g and 9.2 nm, respectively.

Although the wetting characteristics of fibrous membrane play an important role in the process of adsorption, they are not considered as primary factor.[64-67] If the fibrous membrane does not permit penetration of polluted water, the reaction takes place only on the surface of the fiber, resulting in lower adsorption capacity. As a proof of concept, recent report well demonstrated that water-dispersibility nature of the adsorbent enhances the adsorption of alizarin red in the aqueous solution because their wettability nature facilities the pores much more accessible to the adsorbates.[68] We have paid more attention on studying the interaction between fibrous mat and water and their transport behavior to improve the overall removal capacity of metal ions. Until now, limited attention has been paid on liquid moisture transport behaviors of electrospun fibrous membrane especially when they are considering for removal of metal ions. It has been observed that various surface modification processes can be used to design the wetting behavior of fibrous membrane.[69-73]

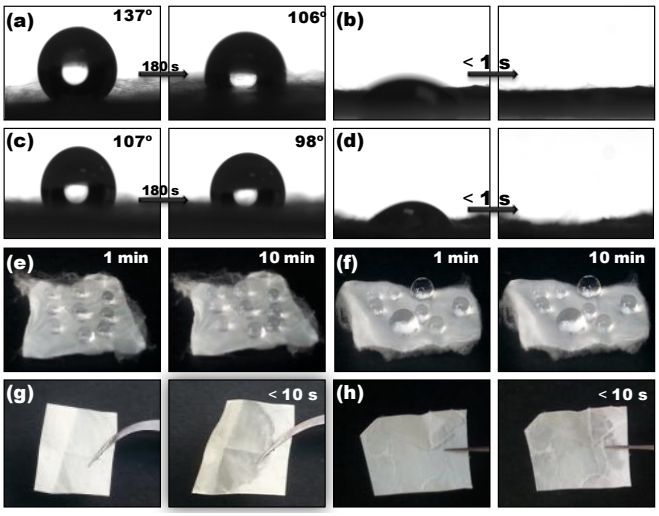

Fig. 3 Wetting behavior of water on porous and nonporous cellulose acetate fibrous membrane before and after encapsulation of AuNC. Contact angle of (a) pCAFM (b) pCAFM/AuNC (c) nCAFM, and (d) nCAFM/AuNC. The contact angle of both pCAFM/AuNC and nCAFM/AuNC suddenly drops down to zero within seconds, followed by the water droplets spreads out and permeates into the membrane. Water droplet was set to 5 μL during the contact angle measurement. Photograph of water droplet on the (e) pCAFM, (f) nCAFM, (g) pCAFM/AuNC and (h) nCAFM/AuNC. The wet zone in pCAFM/AuNC and nCAFM/AuNC represents the spreading of water droplet.

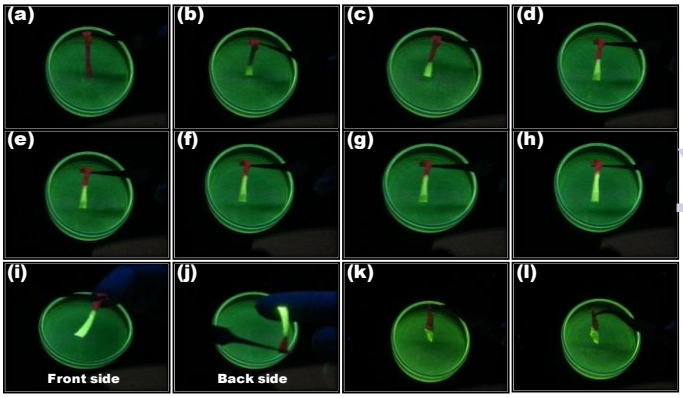

Fig. 4 (a-h) A sequence of frames showing the propagation of water upward in the pCAFM/AuNC strip. The red and green color represents the characteristics of AuNC and FITC dye. (i & j) Front and back side of pCAFM/AuNC after spread out of water. The water is efficiently diffused into the membrane, confirmed from the back side of the membrane emitting green fluorescence due to the presence of transported FITC dye (k & l) photograph of nCAFM/AuNC showing the propagation of water after 30 s and 2 min, respectively.

Further, we are gratified at presenting the primary report here talking about the enhanced wetting characteristics and capillary action of electrospun porous cellulose acetate fibrous membrane (pCAFM) and nonporous cellulose acetate fibrous membrane (nCAFM) by encapsulating AuNC. In depth information on the wettability nature and the diffusion ability of water in pCAFM and nCAFM before and after coating with AuNC is taken from the time dependent contact angles. The contact angle of pristine pCAFM and nCAFM is measured to be 137° and 106°, respectively, which is found to decrease to 107° and 98° after 3 minutes as shown in Fig. 3a and c. It is found that the roughness is the inducing factor behind the increase in the water contact angle of pCAFM. Interestingly, it is also noticed that the contact angle of both pCAFM/AuNC and nCAFM/AuNC suddenly drops down to zero, followed by the water droplets spreads out and permeates into the membrane, once it comes into contact with the membrane surface (See Fig. S1). This is confirmed in Fig. 3b and d, showing the capability of incorporating AuNC modifying the

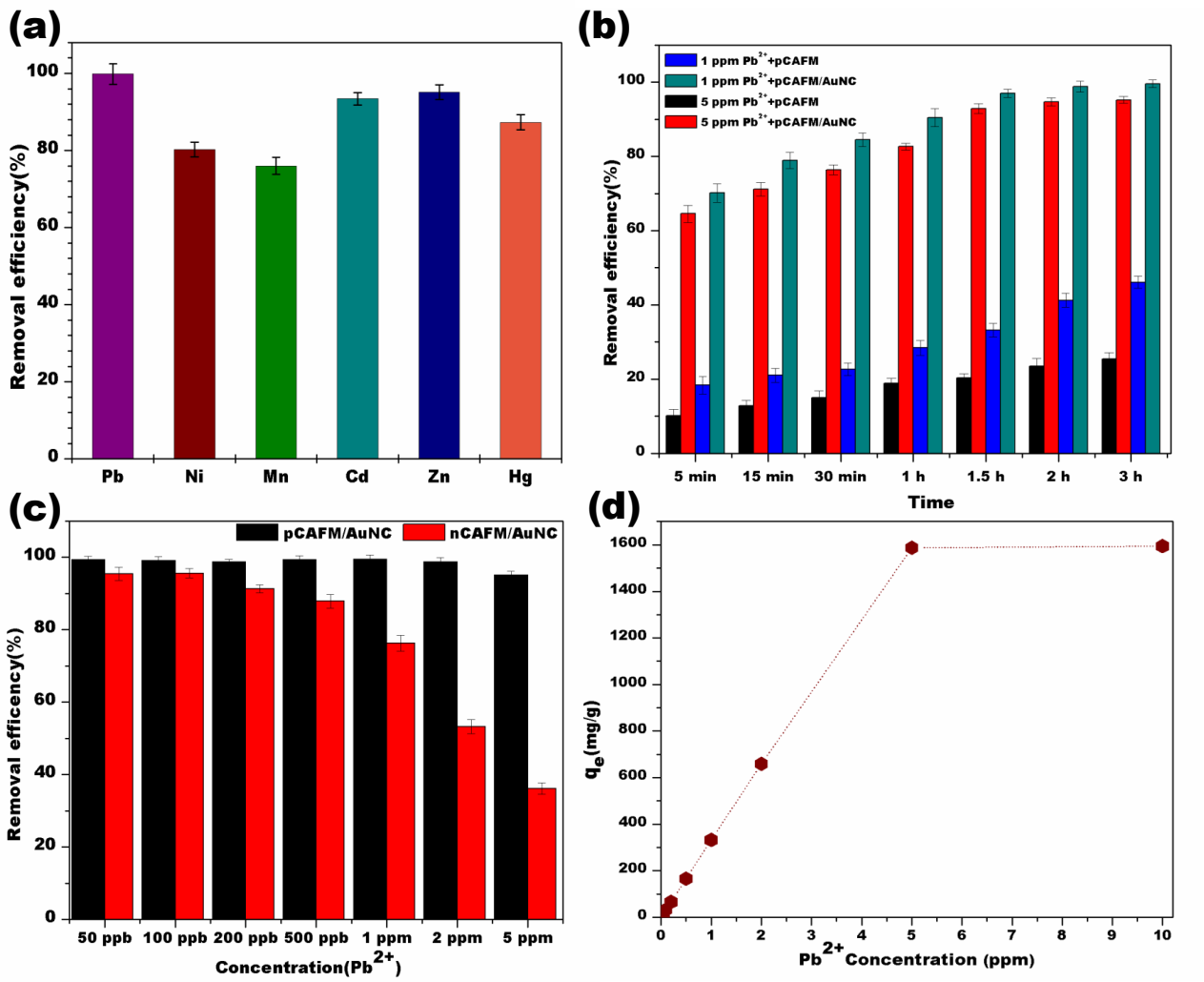

Fig. 5 (a) Removal efficiency of toxic metal ions (Pb^{2+}, Ni^{2+}, Mn^{2+}, Cd^{2+}, Zn^{2+} and Hg^{2+}) using pCAFM/AuNC in water. The pCAFM/AuNC has the ability to remove the metal ions in the order of Pb^{2+}>Zn^{2+}>Cd^{2+}>Hg^{2+} >Ni^{2+}>Mn^{2+}. The concentration is set to 1 ppm for all metal ions (b) Time dependent removal efficiency of Pb^{2+} at 1ppm and 5 ppm concentrations. (c) Effect of initial concentration of Pb^{2+} for removal efficiency of pCAFM/AuNC and their comparative removal efficiency with nCAFM/AuNC. (d) Adsorption capacity for pCAFM/AuNC.

surface characteristics, from hydrophobic to hydrophilic. Fig. 3e-h further demonstrates the real time wettability nature of the fibrous membrane by placing a few drops of water on their surface.

The diffusion of water droplet is uniform in all direction at fraction of seconds whereas the water droplet is stable on the pristine membrane. The above stated fact has been clearly supported by evidence from the measured contact angle. Notably, immediate water diffusion is happened in pCAFM/AuNC as compared with nCAFM/AuNC, which could be attributed to stronger capillary effect induced by large volume of pores present in the fibers. This is further confirmed that the porous structure is well maintained post decorating AuNC. On exposure to UV light (λ_{ext}-366 nm), both AuNC and Fluorescein isothiocyanate (FITC) dye emit red and green fluorescence, respectively. Thus, we have combined these efficient attributes to perform an experiment for demonstrating the capillary motion induced liquid transport behavior in the pCAFM/AuNC and nCAFM/AuNC as illustrated in Fig. 4. In addition, the fast propagation of water in pCAFM/AuNC is supported by Video S1.

The experiment started with dipping a piece of pCAFM/AuNC strip in water containing FITC dye, and transport of water was monitored under UV light. Captivating photographs within 10 seconds of reaction time highlighted the propagation of water upward in the pCAFM/AuNC, comprehensibly demonstrating the green emission of FITC as in Fig. 4 a-h. Remarkably, the diffusion has been found to be uniform on the surface and the bottom of the fibers, confirmed from the back side of the membrane emitting green fluorescence due to the presence of transported FITC dye (Fig. 4i and j). It is interesting to note that the transport rate of

water containing FITC dye in pCAFM/AuNC is significantly higher than the nCAFM/AuNC (Fig. k and l). Also, limitability is observed in the transport of FITC dye in nCAFM/AuNC to an extent. Even after a prolonged period of time, no markable diffusion of water was noticed. Significant improvement is expected from the nanoporous channels to greatly increase the capillary motion and aid water
transport. Hence, this proves the ability of the porous structure of fibers to determine their wetting and transport nature. As seen from the experiment, it is understand that the immersion of membrane in water did not alter the integrity of the membrane structure. The anchored AuNC is found to tightly bind on the wall of the pore, combined with the formation of a strong concrete wall making them stable against swelling. Initially, the adsorption efficiency of pCAFM/AuNC was evaluated against various toxic metal ions such as Pb^{2+}, Ni^{2+}, Mn^{2+}, Cd^{2+}, Zn^{2+} and Hg^{2+}, at 1 ppm concentration as shown in Fig. 5a. Interestingly, the pCAFM/AuNC has the ability to remove the metal ions in the order of Pb^{2+}> Zn^{2+} >Cd^{2+}>Hg^{2+} >Ni^{2+} >Mn^{2+}. The results showed a higher degree of removal efficiency towards Pb^{2+} when compared to other metal ions. Thus, this shifted our focus towards investigating about the feasibility of using designed nanotraps as an adsorbing substrate against the removal of Pb^{2+} in water. The removal efficiency as a function of contact time has been studied and shown in Fig. 5b. The pCAFM has been used as a control. The resulting outcome suggests the removal of ~70% of Pb^{2+} within 5 minutes, and the removing efficiency gradually increases and reached 99% within 3h.

The obtained result prompted us to keep 3 h as the contact time for the following experiments to achieve complete equilibrium. At low concentrations, it is presumed that the ideal adsorbent will remove the metal ions. In addition to the high adsorption capacity in relatively high concentration range, pCAFM/AuNC also exhibits an excellent adsorption performance in lower concentration ranges from 50 ppb as illustrated in Fig. 5c. At this concentration, 99% of Pb^{2+} is removed from the water. The removal efficiency as a function

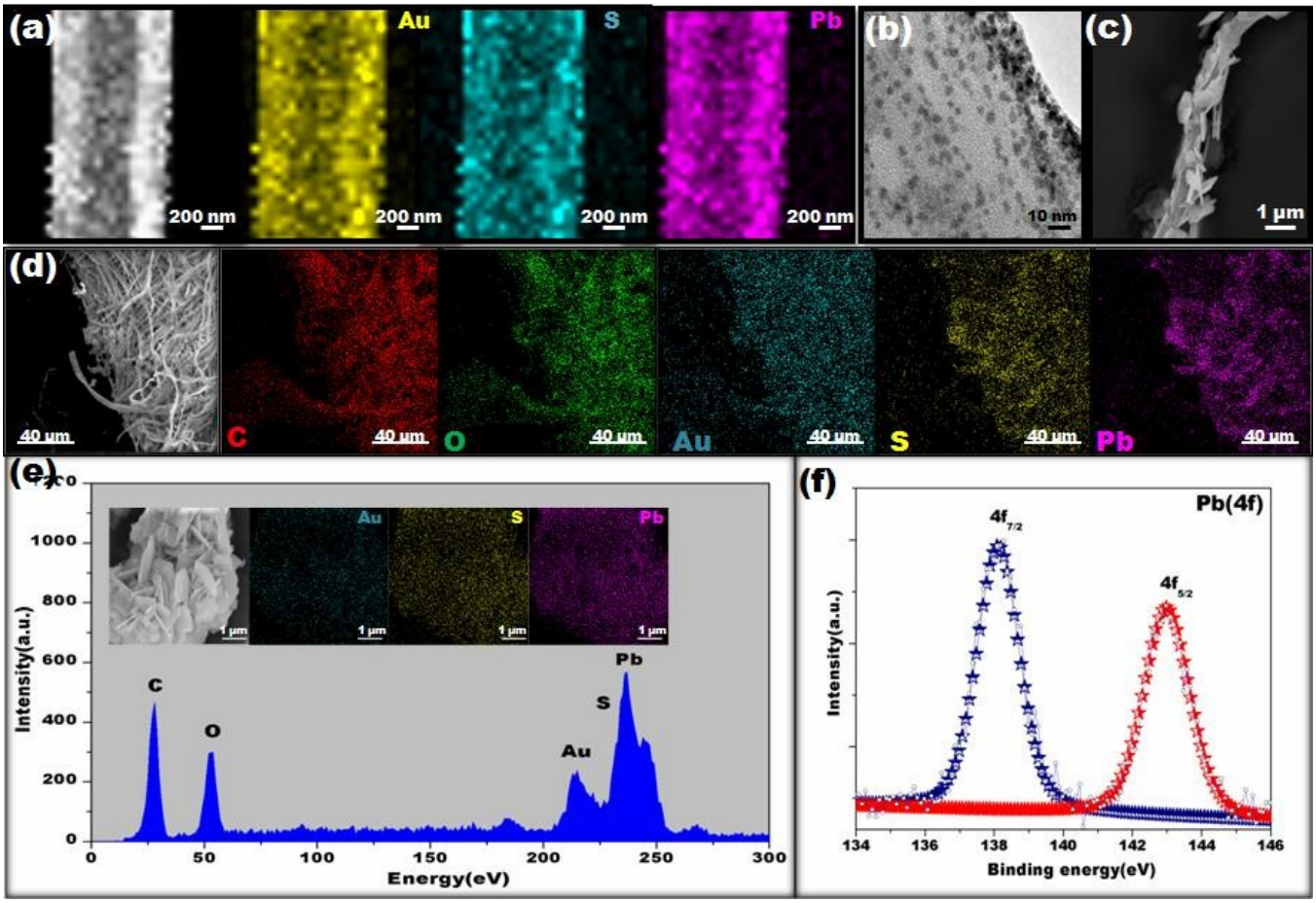

Fig. 6 Investigation on Pb^{2+} binding interaction. (a) HAADF-STEM image and corresponding elemental mapping images of pCAF/AuNC after treatment with 10 ppm Pb^{2+}. (b) TEM images of adsorbed Pb^{2+} on pCAF/AuNC. (c) SEM image of single pCAF/AuNC treated with 50 ppm Pb^{2+}. The adsorbed Pb^{2+} ions are formed as crystal on surface of fibers. (d) SEM image and elemental mapping of pCAFM/AuNC treated with 50 ppm Pb^{2+}. (e) and their EDX spectra. The inset shows the adsorbed Pb^{2+} crystals and their elemental mapping images. (f) XPS spectra of Pb(4f) adsorbed on pCAFM/AuNC.

of Pb^{2+} concentration represents a decrease in the adsorption capacity with increasing the Pb^{2+} concentration. The comparative removing efficiency of pCAFM/AuNC with nCAFM/AuNC are preformed and presented in Fig. 5c. At lower concentration, it is observed that nCAFM/AuNC exhibit good ability for removing the metal ions because the process might be due to surface adsorption. An increase in the concentration from 1 ppm to 5 ppm, notices a solid efficiency decrease, due to limited adsorption sites available for uptake of metal ions.

The resulting outcome has proved that pCAFM/AuNC show higher uptake capabilities than nCAFM/AuNC. The adsorption capacity of pCAFM/AuNC for Pb^{2+} has been studied and the results are shown in Fig. 5d. The enhanced uniform encapsulation of AuNC inside the porous structure and their active interaction with metal ions leads to maximum adsorption capacity of Pb^{2+} which is found to go as high as 1587 mg/g. Here, we list down the reasons behind the ability of pCAFM/AuNC to exhibit such high adsorption capacity. Firstly, the ability of the porous structure to showcase high loading encapsulation of non-aggregated AuNC, following improved interaction with metal ions. Secondly, the well maintained nanopore channels post encapsulation efficiently facilitate better water permeation without losing their physical structure. And further, large surface area, abundant inter accommodations and well dispersed AuNC in nanopores forms a nanotraps which provides increased active sites for adsorption. The discussed method has also shown that the diffusion of Pb^{2+} into the pCAF/AuNC is equivalent to the penetration depth of AuNC is clearly shown in Fig. 6a. The metal ions are found to have a strong bond with DTT, which binds to the gold surface through Au-S bonds.[74,75]

When the membrane comes into contact with the water, the metal ions are rapidly penetrated and adsorbed on the surface of AuNC as confirmed by EDS line profile of Au, S, and Pb as clearly seen in Fig. S2. The TEM image of the pCAF/AuNC surface after adsorption of Pb^{2+} evidenced that the adsorption did not induce the aggregation of AuNC (see Fig. 6b). The morphology of pCAFM/AuNC after adsorption of Pb^{2+} have been studied and the results reveal the formation of crystals on the surface when the concentration reaches 50 ppm as illustrated in Fig. 6c-d. The EDX spectra and mapping of formed crystals shown in Fig. 6e. The interaction of AuNC upon addition of different concentrations of Pb^{2+} (50 ppb, 1 ppm, 10 ppm, 20 ppm and 50 ppm) has been studied by UV-vis spectra and their fluorescence characteristics has been observed under UV light (shown as inset Fig. S3). Precisely, it is noticed that no change is observed at low concentrations, while there is an emergence of a new peak at around 280 nm corresponding to the strong complexation between DTT and Pb^{2+}. Expectedly, there was nil fluorescence decrease with any of the tested concentrations. However, on adding 50 ppm solution to the AuNC solution, the bottom of the vial showed the formation of a precipitate owing to a strong complex formation between Pb^{2+} and DTT. As can be seen from the Fig. S3, even after formation of precipitate the AuNC emits red fluorescence which revealing the unaffected nature of AuNC by Pb^{2+}. This is found to be the underlying mechanism for the observed adsorption efficiency for Pb^{2+} ions, because a similar type of crystal formation has not been seen with any other metal ions even at the higher concentration as seen Fig. S4.

The information on the chemical state of pCAFM/AuNC (S from DTT and Au from AuNC) before and after adsorption of Pb^{2+} has been studied using XPS spectra as shown in Fig. S5 a and b. The observed two peaks at 162.5 eV and 163.7 eV corresponds to the S-Au covalent bond, confirms the successful preparation of thiol bound gold nanocluster and free SH groups.[76] Upon interaction with Pb^{2+} (10 ppm), there is no change in chemical state of the S and Au. The adsorbed Pb^{2+} has been confirmed by taking XPS spectra on pCAFM/AuNC surface (Fig. 6f). Further, adsorption of other metal ions on the pCAFM/AuNC surface was also analyzed by XPS (Fig. S6). In addition, EDX mapping (Fig. S7) confirms the uniform adsorption of metal ions over the membrane surface owing to the formation of metal ion complexes with DTT molecule since it contains donor groups which are highly capable of making complexes. The detailed investigation confirms that the formation of nanotraps and their ability to capture toxic pollutants inside their cavity makes up for an environmentally safe adsorbent.

Conclusions

To conclude, we have devised a simple and effective approach to create stable nanotraps for the effective capturing of toxic metal ions in water. The obtained pCAFM/AuNC containing huge nanotraps, exhibited abundant adsorption sites for metal ions, resulting in high extraction capacity upto 1587 mg/g for Pb^{2+}. Post encapsulation of AuNC, the porous nature of pCAFM/AuNC seems to be maintained well. Interestingly, it has been found that the occurrence of pores greatly enhances the capillary effect of pCAFM/AuNC when compared to the nCAFM/AuNC. In addition, the facile penetration ability of Pb^{2+} into pCAF/AuNC forms a complex with AuNC based on its availability, resulting in the formation of a crystal. This emerges as the primary reason for attaining high adsorption capacity. The comparative attribute of pCAF/AuNC with nCAF/AuNC paves the way for excellent stability, porous structure and capillary effect for enhanced removal capacity. The study described here opens up a new path towards preparing a stable composite membrane containing vast nanotraps without comprising or losing their parent properties of adsorbent.

Acknowledgements

A.S. acknowledges The Scientific & Technological Research Council of Turkey (TUBITAK), BIDEB 2221-Fellowships for Visiting Scientists and Scientists on Sabbatical for the fellowship. B.B. thanks (TUBITAK-BIDEB 2216, Research Fellowship Programme for Foreign Citizens) for postdoctoral fellowship. A.C. acknowledges TUBITAK (project No: 113Y348) for postdoctoral funding. T.U. acknowledges FP7-Marie Curie International Reintegration Grant (IRG) for funding NANOWEB

(PIRG06-GA-2009-256428). T.U also acknowledges The Turkish Academy of Sciences - Outstanding Young Scientists Award Program (TUBA-GEBIP). Authors thank M. Guler and Dr Gokçe Çelik for TEM-STEM and ICP-MS technical support, respectively.

Notes and references

1 L. Jarup, *Br. Med. Bull.*, 2003, **68**, 167–182.
2 EPA, U.S., Drinking Water Contaminants, http://water.epa.gov/drink/contaminants/index.cfm, accessed on 07 10 15.
3 M. A. Hashim, S. Mukhopadhyay, J. N. Sahu and B. Sengupta, *J. Environ. Manage.*, 2011, **92**, 2355–2388.
4 X.-F. Yu, J.-W. Liu, H.-P. Cong, L. Xue, M. N. Arshad, H. A. Albar, T. R. Sobahi, Q. Gao and S.-H. Yu, *Chem. Sci.*, 2015, **6**, 2511–2515.
5 P. A. Turhanen, J. J. Vepsäläinen and S. Peräniemi, *Sci. Rep.*, 2015, **5**, 8992.
6 M. A. Shannon, P. W. Bohn, M. Elimelech, J. G. Georgiadis, B. J. Mariñas and A. M. Mayes, *Nature*, 2008, **452**, 301–310.
7 M. A. Barakat, *Arab. J. Chem.*, 2011, **4**, 361–377.
8 H. Y. Yang, Z. J. Han, S. F. Yu, K. L. Pey, K. Ostrikov and R. Karnik, *Nat. Commun.*, 2013, **4**, 2220.
9 I. Ali, *Chem. Rev.*, 2012, **112**, 5073–5091.
10 R. Liu, F. Liu, C. Hu, Z. He, H. Liu and J. Qu, *J. Hazard. Mater.*, 2015, **300**, 847–854.
11 B. Alies, J. D. Wiener and K. J. Franz, *Chem. Sci.*, 2015, **6**, 3606–3610.
12 D. E. Salt, M. Blaylock, N. P. Kumar, V. Dushenkov, B. D. Ensley, I. Chet and I. Raskin, *Biotechnology*, 1995, **13**, 468–474.
13 I. Ali and V. K. Gupta, *Nat. Protoc.,* 2006, **1**, 2661–2667.
14 I. Ojea-Jiménez, X. López, J. Arbiol and V. Puntes, *ACS Nano*, 2012, **6**, 2253–2260.
15 A. M. López_Marzo, J. Pons and A. Merkoçi, *J. Mater. Chem. A*, 2014, **2**, 8766–8772.
16 Y. C. Shih, C. Y. Ke, C. J. Yu, C. Y. Lu and W. L. Tseng, *ACS Appl. Mater. Interfaces*, 2014, **6**, 17437–17445.
17 J. Trujillo-Reyes, J. R. Peralta-Videa and J. L. Gardea-Torresdey, *J. Hazard. Mater.*, 2014, **280**, 487–503.
18 J. Zhao, X. Zhang, X. He, M. Xiao, W. Zhang and C. Lu, *J. Mater. Chem. A*, 2015, **3**, 14703–14711.
19 H. Ma, B. S. Hsiao and B. Chu, *ACS Macro Lett.*, 2012, **1**, 213–216.
20 G. Hong, X. Li, L. Shen, M. Wang, C. Wang, X. Yu and X. Wang, *J. Hazard. Mater.*, 2015, **295**, 161–169.
21 Y. Lin, W. Cai, X. Tian, X. Liu, G. Wang and C. Liang, *J. Mater. Chem.*, 2011, **21**, 991–997.
22 D. Yang, Z. Zheng, H. Liu, H. Zhu, X. Ke, Y. Xu, D. Wu and Y. Sun, *J. Phys. Chem. C*, 2008, **112**, 16275–16280.
23 P. Kampalanonwat and P. Supaphol, *ACS Appl. Mater. Interfaces*, 2010, **2**, 3619–3627.
24 W. Xu, J. Wang, L. Wang, G. Sheng, J. Liu, H. Yu and X.-J. Huang, *J. Hazard. Mater.*, 2013, **260**, 498–507.
25 J. Yang, H. Zhang, M. Yu, I. Emmanuelawati, J. Zou, Z. Yuan and C. Yu, *Adv. Funct. Mater.,* 2014, **24**, 1354–1363.
26 M. X. Tan, Y. N. Sum, J. Y. Ying and Y. Zhang, *Energy Environ. Sci.*, 2013, **6**, 3254–3259.
27 L. Kong, L. Yan, Z. Qu, N. Yan and L. Li, *J. Mater. Chem. A*, 2015, **3**, 15755–15763.
28 Y. Xie, J. Wang, M. Wang and X. Ge, *J. Hazard. Mater.*, 2015, **297**, 66–73.
29 X. Feng, G. E. Fryxell, L.-Q. Wang, A. Y. Kim, J. Liu and K. M. Kemner, *Science*, 1997, **276**, 923–926.
30 D. Wu, F. Xu, B. Sun, R. Fu, H. He and K. Matyjaszewski, *Chem. Rev.,* 2012, **112**, 3959−4015.
31 Z. Li, D. Wu, Y. Liang, R. Fu and K. Matyjaszewski, *J. Am. Chem. Soc.,* 2014, **136**, 4805−4808.
32 L. J. Prins, *Acc. Chem. Res.*, 2015, **48**, 1920–1928.
33 C. Pezzato, S. Maiti, J. L.-Y. Chen, A. Cazzolaro, C. Gobbo and L. J. Prins, *Chem. Commun.*, 2015, **51**, 9922–9931.
34 A. Senthamizhan and T. Uyar, in *Electrospinning for High Performance Sensors*, ed. A. Macagnano, E. Zampetti and E. Kny, Springer International Publishing, Switzerland, 1st edn., 2015, Ch. 8, pp. 179-204.
35 X.-H. Zhang, T.-Y. Zhou and X. Chen, *Chinese J. Anal. Chem.*, 2015, **43**, 1296–1305.
36 J. Sun and Y. Jin, *J. Mater. Chem. C*, 2014, **2**, 8000–8011.
37 A. Senthamizhan, A. Celebioglu and T. Uyar, *Chem. Commun.*, 2015, **51**, 5590–5593.
38 A. Senthamizhan, A. Celebioglu and T. Uyar, *J. Mater. Chem. A*, 2014, **2**, 12717–12723.
39 A. Senthamizhan, A. Celebioglu and T. Uyar, *Sci. Rep.*, 2015, **5**, 10403.
40 Y. Zhai, N. Wang, X. Mao, Y. Si, J. Yu, S. S. Al-Deyab, M. El-Newehy and B. Ding, *J. Mater. Chem. A*, 2014, **2**, 14511–14518.
41 S. Anitha, B. Brabu, K. P. Rajesh and T. S. Natarajan, *Mater. Lett.*, 2013, **92**, 417–420.
42 T. Uyar, R. Havelund, J. Hacaloglu, Ḱ. F. Besenbacher and P. Kingshott, *ACS Nano,* 2010, **4**, 5121–5130.
43 A. Senthamizhan, A. Celebioglu, S. Bayir, M. Gorur, E. Doganci, F. Yilmaz and T. Uyar, *ACS Appl. Mater. Interfaces*, 2015, **7**, 21038–21046.
44 V. Thavasi, G. Singh and S. Ramakrishna, *Energy Environ. Sci.*, 2008, **1**, 205–221.
45 S. Anitha, B. Brabu, D. J. Thiruvadigal, C. Gopalakrishnan and T. S. Natarajan, *Adv. Sci. Lett.,* 2012, **5**, 468–474.
46 A. Senthamizhan, B. Balusamy and T. Uyar, *Anal. Bioanal. Chem.,* (DOI: 10.1007/s00216-015-9152-x).
47 A. Senthamizhan, B. Balusamy, Z. Aytac and T. Uyar, *Anal. Bioanal. Chem.,* (DOI: 10.1007/s00216-015-9149-5).
48 S. Anitha and T. S. Natarajan, *J. Nanosci. Nanotechnol.,* 2013, **13**, 4256–4264.
49 S. Anitha, D. J. Thiruvadigal and T. S. Natarajan, *Mater. Lett.*, 2011, **65**, 2872–2876.
50 Z. M. Huang, Y. Z. Zhang, M. Kotaki and S. Ramakrishna, *Compos. Sci. Technol*., 2003, **63**, 2223–2253.
51 L. Persano, A. Camposeo, C. Tekmen and D. Pisignano, *Macromol. Mater. Eng*., 2013, **298**, 504–520.
52 W. E. Teo and S. Ramakrishna, *Nanotechnology*, 2006, **17**, R89–R106.
53 R. Sahay, P. S. Kumar, R. Sridhar, J. Sundaramurthy, J. Venugopal, S. G. Mhaisalkar and S. Ramakrishna, *J. Mater. Chem*., 2012, **22**, 12953–12971.
54 D. Kai, S. S. Liow and X. J. Loh, *Mater. Sci. Eng. C*, 2014, **45**, 659–670.
55 S. Cavaliere, S. Subianto, I. Savych, D. J. Jones and J. Rozière, *Energy Environ. Sci*., 2011, **4**, 4761–4785.
56 K. A. Rieger, N. P. Birch and J. D. Schiffman, *J. Mater. Chem. B*, 2013, **1**, 4531–4541.
57 A. Celebioglu and T. Uyar, *Mater. Lett.*, 2011, **65**, 2291–2294.
58 H. Ding, C. Liang, K. Sun, H. Wang, J. K. Hiltunen, Z. Chen and J. Shen, *Biosens. Bioelectron.*, 2014, **59**, 216–220.
59 A. Senthamizhan, A. Celebioglu, B. Balusamy and T. Uyar, *Sci. Rep*., 2015, **5**, 15608.
60 A. Kr zel, W. Lesniak, M. Jezowska-Bojczuk, P. Mlynarz, J. Brasuñ, H. Kozlowski and W. Bal, *J. Inorg. Biochem.,* **84**, 77–88.

61 A. Gupta, A. Chaudhary, P. Mehta, C. Dwivedi, S. Khan, N. C. Verma and C. K. Nandi, *Chem. Commun.*, 2015, **51**, 10750–10753.
62 A. Chaudhary, C. Dwivedi, M. Chawla, A. Gupta and C. K. Nandi, *J. Mater. Chem. C*, 2015, **3**, 6962–6965.
63 J. Zhang, Y. Yuan, G. Liang, M. N. Arshad, H. A. Albar, T. R. Sobahi and S.-H. Yu, *Chem. Commun.*, 2015, **51**, 10539–10542.
64 J. A. Prince, D. Rana, T. Matsuura, N. Ayyanar, T. S. Shanmugasundaram and G. Singh, *Sci. Rep.*, 2014, **4**, 6949.
65 M. Tao, L. Xue, F. Liu and L. Jiang, *Adv. Mater.*, 2014, **26**, 2943–2948.
66 J. J. Alcaraz-Espinoza, A. E. Chávez-Guajardo, J. C. Medina-Llamas, C. A. S. Andrade and C. P. de Melo, *ACS Appl. Mater. Interfaces*, 2015, **7**, 7231–7240.
67 J. Yuan, X. Liu, O. Akbulut, J. Hu, S. L. Suib, J. Kong and F. Stellacci, *Nat. Nanotechnol.*, 2008, **3**, 332–336.
68 W. Mai, B. Sun, L. Chen, F. Xu, H. Liu, Y. Liang, R. Fu, D. Wu and K. Matyjaszewski, *J. Am. Chem. Soc.,* 2015, **137**, 13256−13259.
69 M. Lejuene, L. M. Lacroix, F. Bretagnol, A. Valsesia, P. Colpo and F. Rossi, *Langmuir*, 2006, **22**, 3057–3061.
70 S. Anitha, B. Brabu, D. J. Thiruvadigal, C. Gopalakrishnan and T. S. Natarajan, *Carbohydr. Polym.*, 2013, **97**, 856–863.
71 X. Lu, J. Zhou, Y. Zhao, Y. Qiu and J. Li, *Chem. Mater.*, 2008, **20**, 3420–3424.
72 A. Li, H.-X. Sun, D.-Z. Tan, W.-J. Fan, S.-H. Wen, X.-J. Qing, G.-X. Li, S.-Y. Li and W.-Q. Deng, *Energy Environ. Sci.*, 2011, **4**, 2062–2065.
73 M. Guo, B. Ding, X. Li, X. Wang, J. Yu and M. Wang, *J. Phys. Chem. C*, 2010, **114**, 916–921.
74 C. Xiao, X. Zhang, J. Liu, A. Yang, H. Zhao, X. Li, Y. He and Z. Yuan, *Anal. Methods*, 2015, **7**, 924–929.
75 J. Y. Kim and J. S. Lee, *Nano Lett.*, 2009, **9**, 4564–4569.
76 D.-H. Tsai, T. J. Cho, F. W. DelRio, J. M. Gorham, J. Zheng, J. Tan, M. R. Zachariah and V. A. Hackley, *Langmuir*, 2014, **30**, 3397–3405.

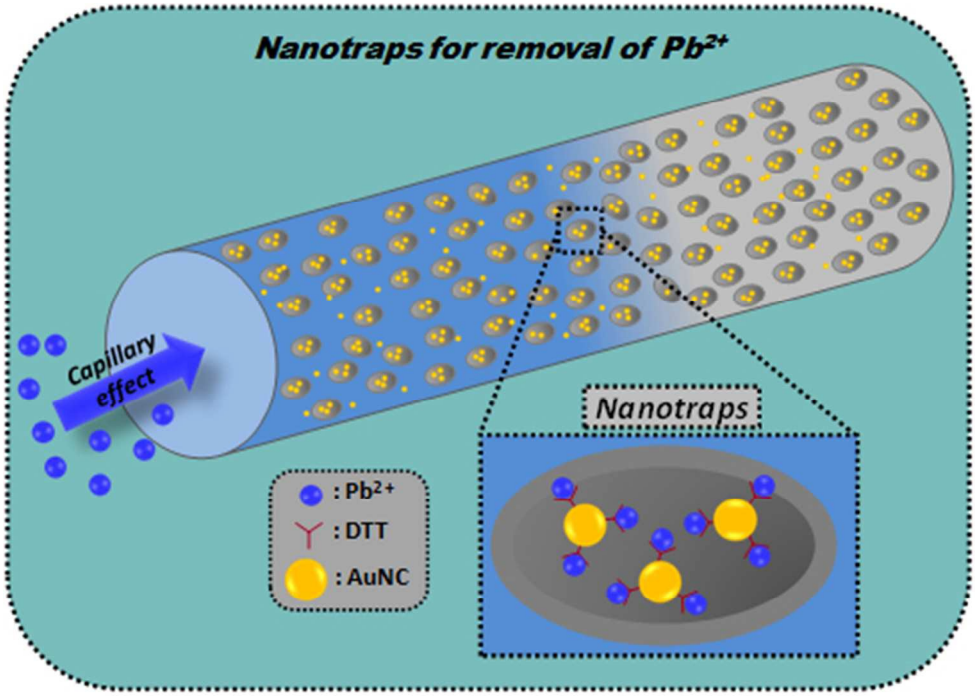

41x29mm (300 x 300 DPI)